Available online at www.sciencedirect.com
SCIENCE DIRECT®
Journal of Solid State Chemistry 177 (2004) 4665–4671
JOURNAL OF SOLID STATE CHEMISTRY
www.elsevier.com/locate/jssc

Rhombohedral-cubic transition in $Li_{0.2}Na_{0.3}La_{0.5}TiO_3$ perovskite

Alejandro Varez[a], Maria T. Fernandez-Díaz[b], Jesus Sanz[c,*]

[a] *Dpt Materials Science and Engineering, Universidad Carlos III de Madrid, E-28911 Leganés, Spain*
[b] *Institut Laue-Langevin, F-38045 Grenoble, France*
[c] *Instituto de Ciencia de Materiales, CSIC, Cantoblanco, E-28049 Madrid, Spain*

Received 24 February 2004; received in revised form 18 June 2004; accepted 23 June 2004

Abstract

High-temperature behavior of the fast ionic conductor $Li_{0.2}Na_{0.3}La_{0.5}TiO_3$ has been investigated by neutron powder diffraction between 300 and 1073 K. The Rietveld analysis of diffraction patterns showed around 1000 K a change from rhombohedral ($R\bar{3}c$) to cubic ($Pm3\,m$) symmetry. During the heating, the tilting of octahedra along the [111] direction of the cubic perovskite decreased and the rhombic distortion of oxygen square windows that relates contiguous A-sites of the perovskite was eliminated. The influence of the octahedral tilting on Li mobility is finally discussed.

Keywords: Lanthanum lithium titanate; High temperature neutron diffraction; Perovskite structure; Rhombohedral-cubic transition

1. Introduction

The discovery of the high ionic conductivity in (Li,La)TiO_3 samples [1,2], with perovskite structure (ABO_3), has triggered off a great deal of research activity to analyze structural features that determine the high mobility of lithium ($\sigma \sim 10^{-3}\,S\,cm^{-1}$ at 300 K). An overview of the chemical composition and crystal structure data reported for this system in the literature can be found in Ref. [3]. However, the actual mechanism of Li conduction is not clearly understood. In these perovskites, La^{3+} ions can be substituted by Li^{+} ions, constituting the solid solution with general formula $Li_{3x}La_{2/3-x}TiO_3$ where the amount of nominal vacant A sites is given by $\square = 1/3-2x$. In these perovskites, the presence of vacancies plays an important role. Li-poor perovskites, $x<0.06$, display an orthorhombic symmetry and the ordering of vacancies in alternate planes favors a two-dimensional mobility of lithium [4,5]. In samples with higher Li contents, $x>0.1$, the ordering of vacancies decreases and the structure becomes tetragonal [6]. Finally, Li-rich samples quenched from high temperature [7–11] adopt a pseudocubic symmetry in which vacancy ordering is removed and Li mobility displays a three-dimensional character.

The use of neutron diffraction (ND) technique is particularly adapted to study the exact position of light elements, like Li and oxygen. Previous studies allowed a precise determination of La–O, Ti–O and O–O distances in $Li_{3x}La_{2/3-x}\,TiO_3$ perovskites [12–16]. The unusual Li location at unit cell faces of the perovskites permit to understand high Li conductivity values of this series. In particular, partially occupied Li (1/6) and La (1/2) sites of the $Li_{0.5}La_{0.5}TiO_3$ end member, supply an interconnected pathway for the Li diffusion. On the other hand, Li conductivity decreased drastically when Li was substituted by Na ions in $Li_{0.5-x}Na_xLa_{0.5}TiO_3$ perovskites [17,18]. This fact was interpreted on the basis of percolation theory, assuming that Na ions occupy A-sites and Li ions occupy faces of the perovskite unit cell. According to this fact, the number of vacant A-sites is

*Corresponding author. Departamento de Sólidos Iónicos, Instituto de Ciencia de Materiales Cantoblanco, 28049 Madrid, Spain. Fax: +34-91-372-06-23.
E-mail address: jsanz@icmm.csic.es (J. Sanz).

0022-4596/$ - see front matter © 2004 Elsevier Inc. All rights reserved.
doi:10.1016/j.jssc.2004.06.037

reduced with the Na content, decreasing drastically the conductivity when the amount of vacancies approached the percolation threshold, $n_v = 0.31$.

In the present paper, we report a detailed neutron diffraction (ND) investigation of structural changes produced in the $Li_{0.2}Na_{0.3}La_{0.5}TiO_3$ perovskite in the temperature range 300–1073 K. In particular, changes produced during heating in LaO_{12} and TiO_6 polyhedra, disposition of octahedra and oxygen square windows have been analyzed. Finally, the influence of detected modifications on transport properties of perovskites is discussed.

2. Experimental

The $Li_{0.2}Na_{0.3}La_{0.5}TiO_3$ sample was prepared by solid state reaction of a stoichiometric mixture of high-purity $^7LiOH \cdot H_2O$, Na_2CO_3, La_2O_3 and TiO_2 reagents [17,18]. Na and Li losses produced during calcinations were minimized using slow heating rates (1°/min). Pellets of the calcinated powder were finally fired at 1600 K in air for 6 h, and quenched in liquid nitrogen. The final chemical composition of the sample was evaluated through inductively coupled plasma spectroscopy (ICP) using a JY-70 plus spectrometer. For that, the sample was dissolved by digestion with H_2SO_4 and $(NH_4)_2SO_4$. The homogeneity of the sample was tested by means of a Philips XL30 Scanning Electron Microscope equipped with a back-scattered electrons detector (BSE).

X-ray diffraction (XRD) experiments were carried out in a Philips X'Pert automatic diffractometer with ($\theta/2\theta$) Bragg–Brentano geometry, Cu$K\alpha$ radiation and a curved graphite monochromator.

ND patterns were collected in the very high-resolution powder diffractometer D1A at ILL-Grenoble. A wavelength of 1.912 Å was selected from a Ge monochromator. The counting time was 4 h, using about 4 g of sample contained in a vanadium can. ND patterns were recorded in a furnace in the 300–1073 K range. A pseudo-Voigt function was chosen to reproduce the line shape of diffraction peaks in structural refinements. The Rietveld analysis of ND patterns was carried out with the Fullprof program. In this analysis, coherent scattering lengths used for La, Li, Ti and O were 8.24, −1.90, −3.30 and 5.80 fm.

3. Results

XRD and scanning electron microscopy (SEM) analyses of $Li_{0.2}Na_{0.3}La_{0.5}TiO_3$ revealed the high purity of the sample. The room temperature XRD pattern was fitted with a single cubic unit cell ($Pm3m$ S.G.; $a = 3.8601$ Å). Fig. 1a shows the temperature dependence of ND patterns with temperature. Each pattern was collected after 30 min of thermal stabilization, once the furnace temperature was achieved. At room temperature the sample displays the rhombohedral symmetry ($R\bar{3}c$ S.G.; $a = 5.479$ and $c = 13.414$ Å) reported in the quenched $Li_{0.5}La_{0.5}TiO_3$ perovskite [12]. The shift of diffraction peaks towards lower 2θ values, is a consequence of the thermal expansion of the perovskite.

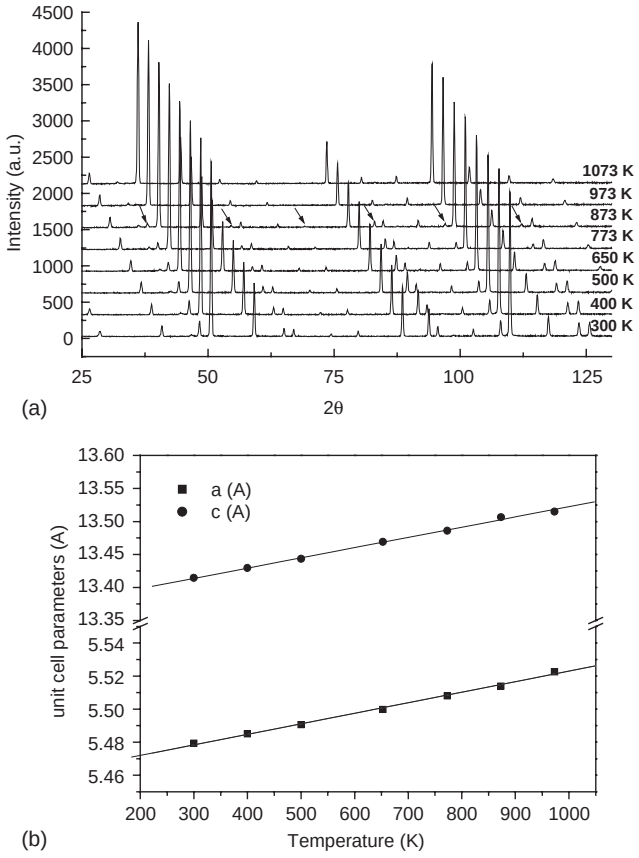

Fig. 1. (a) Neutron diffraction patterns of the $Li_{0.2}Na_{0.3}La_{0.5}TiO_3$ perovskite measured at different temperatures. Each pattern was collected after 30 min of temperature stabilization. Arrows denote rhombohedral superstructure peaks that disappear during sample heating. Indexation of the end perovskite member was carried out considering rombohedral ($R\bar{3}c$) and cubic ($Pm3m$) symmetries. (b) Rhombohedral lattice constants of $Li_{0.2}Na_{0.3}La_{0.5}TiO_3$ perovskite as a function of temperature. The solid lines correspond to the linear fit.

Fig. 1b shows the temperature dependence of the lattice constants deduced from the refinement of diffraction patterns with a hexagonal unit cell ($R\bar{3}c$ S.G.). The lattice parameters increase smoothly with temperature in a linear way. Expansion of lattice parameters was fitted to the relations $a(T) = a_0 + a_1 T$ and $c(T) = c_0 + c_1 T$. The expansion coefficients deduced for a and c parameters are 1.165×10^{-5} and 1.174×10^{-5} K^{-1}. In all the temperature range, the c/a ratio was close to 1, indicating an isotropic expansion of the unit cell.

Above 773 K, intensity of superstructure peaks of the rhombohedral phase decreases progressively with temperature (arrows of Fig. 1a), and finally disappear at 1073 K. Then ND patterns was indexed with the cubic symmetry (*Pm*3*m* S.G.).

The Rietveld analysis of ND patterns showed that La and Na ions are located in A-sites while Li ions occupy the centre of unit cell faces of the perovskite (Tables 1 and 2). In this analysis, the isotropic thermal factor of Na was anchored to that of the La ions. In the case of oxygen atoms, the consideration of anisotropic thermal factors improved considerably figures of merit. As an example of the refinements, Fig. 2 shows fitting of neutron diffraction patterns recorded at 300 and 1073 K, using the rhombohedral and cubic models given in Table 1. Results of ND patterns refinement are given in Table 2. In all cases, agreement factors attained were remarkably good.

Table 1
Positional parameters for rhombohedral and cubic perovskites used in the structural refinement

S.G. $R\bar{3}c$[a]			S.G. *Pm*3*m*		
Atom	Position	Atomic coordinates	Atom	Position	Atomic coordinates
La	6*a*	0, 0, 1/4	La	1*b*	1/2, 1/2, 1/2
Li	18*d*	1/2, 0, 0	Li	3*c*	1/2, 1/2, 0
Ti	6*b*	0, 0, 0	Ti	1*a*	0, 0, 0
O	18*e*	$x \approx 1/2, 0, 1/4$	O	3*d*	1/2, 0, 0

[a]Taken from Ref. [12].

4. Discussion

Low-temperature ND patterns of $Li_{0.2}Na_{0.3}La_{0.5}TiO_3$ displayed rhombohedral symmetry. In this phase La, Na and vacancy are located in A-sites but Li ions occupy the unit cell faces of the perovskite (Table 1). As a consequence of this fact, agreement factors improved appreciably (R_I and R_F) when Li ions were included in the refinement of low temperature phases (300 and 400 K). The rotation of TiO_6 octahedra around the [111] direction ($\phi < 7^\circ$) produces distorted LaO_{12} polyhedra in which three La–O distances, 2.52(3), 2.75(6) and 2.96(3) Å were measured. In this phase, the Goldschmidt tolerance factor, $t = d_{A-O}/\sqrt{2}d_{B-O}$, is 0.995.

4.1. Rhombohedral-cubic transition

The Rietveld analysis of ND patterns showed that Ti–O distances practically do not change with temperature. However, mean La–O distances increase from 2.74 to 2.76 Å in the temperature range 300–1073 K (Fig. 3a). From these considerations, it can be concluded that the increment detected in the tolerance factor is due to the bigger expansion of AO_{12} cubooctahedra (aprox. 3.2%) with respect to that of TiO_6 octahedra (aprox. 0.6%). This effect increases V_A/V_B ratio approaching the ideal value, 5, deduced for perovskites (see Table 3). The same trend is observed in the Goldschmidt tolerance factor, that increases from 0.996 to 1 at increasing temperatures (Fig. 3b). Similar observations were reported by Megaw and Darlington during the analysis of a large number of

Table 2
Refined structural parameters of $Li_{0.2}$ $Na_{0.3}$ $La_{0.5}$ TiO_3 between 300 and 1073 K using the rhombohedral distorted perovskite model ($R\bar{3}c$ space group)

Atom	Parameter	300 K	400 K	500 K	650 K	773 K	873 K	973 K	1073 K (C)	Parameter
La/Na	*B*	0.50(5)	0.73(3)	0.78(4)	1.03(3)	1.14(4)	1.41(4)	1.73(4)	1.82(4)	*B*
La	*occ*	0.167(5)	0.164(6)	0.159(6)	0.162(5)	0.175(10)	0.160(5)	0.159(6)	0.166(6)	*occ*
Na	*occ*	0.090(5)	0.104(6)	0.106(6)	0.100(5)	0.062(10)	0.102(5)	0.104(6)	0.084(6)	*occ*
Li	*B*	9.98	11.04	12.63	16.25	14.40	14.42	19.20	20.21	*B*
	occ	0.067	0.067	0.067	0.067	0.067	0.067	0.067	0.067	*occ*
Ti	*B*	0.79(3)	0.79(3)	0.84(4)	1.00(3)	1.21(4)	1.25(3)	1.39(4)	1.39(4)	*B*
O1	*x/a*	0.5399(6)	0.5386(6)	0.5359(6)	0.5320(7)	0.5255(8)	0.5200(9)	0.507(1)	—	*x/a*
	B^a	1.23	1.41	1.55	1.85	2.35	2.51	2.97	2.97(8)	*B*
a (Å)		5.4794 (2)	5.4850 (2)	5.4907 (3)	5.4997 (4)	5.5080 (5)	5.5138 (8)	5.5224 (4)	3.9085 (1)	*a*(Å)
c (Å)		13.414 (1)	13.430 (1)	13.443 (1)	13.469 (2)	13.485 (3)	13.507 (4)	13.515 (2)	—	*c*(Å)
V (Å^3)		348.78 (4)	349.91 (4)	350.98 (5)	352.80 (6)	354.31 (8)	355.6 (1)	356.95 (7)	59.707(3)	*V*(Å^3)
c/a		0.99965	0.99976	0.99979	1.00002	0.99979	1.00021	0.99928	—	*c/a*
	R_I	1.55	1.56	1.86	1.80	1.73	1.24	2.09	1.09	R_I
	R_F	1.09	0.95	1.29	1.23	1.68	0.93	2.63	0.88	R_F
	R_P	5.66	5.54	5.66	5.52	4.96	4.95	4.95	4.63	R_P
	R_{WP}	8.20	8.13	8.20	8.07	7.51	7.28	7.47	6.96	R_{WP}
	R_{exp}	3.86	3.89	3.96	4.01	4.06	4.11	4.19	3.56	R_{exp}
	χ^2	1.97	1.71	1.59	1.56	1.97	1.39	1.32	1.35	χ^2

At the highest temperature, the cubic *Pm*3*m* model was used.
[a]$B_{equi} = 4/3[a_1{*}a_1{*}\beta_{11} + a_2{*}a_2{*}\beta_{22} + c{*}c{*}\beta_{33} + a_1{*}a_2{*}\beta_{12} + a_1{*}c{*}\beta_{13} + a_2{*}c{*}\beta_{23}]$.

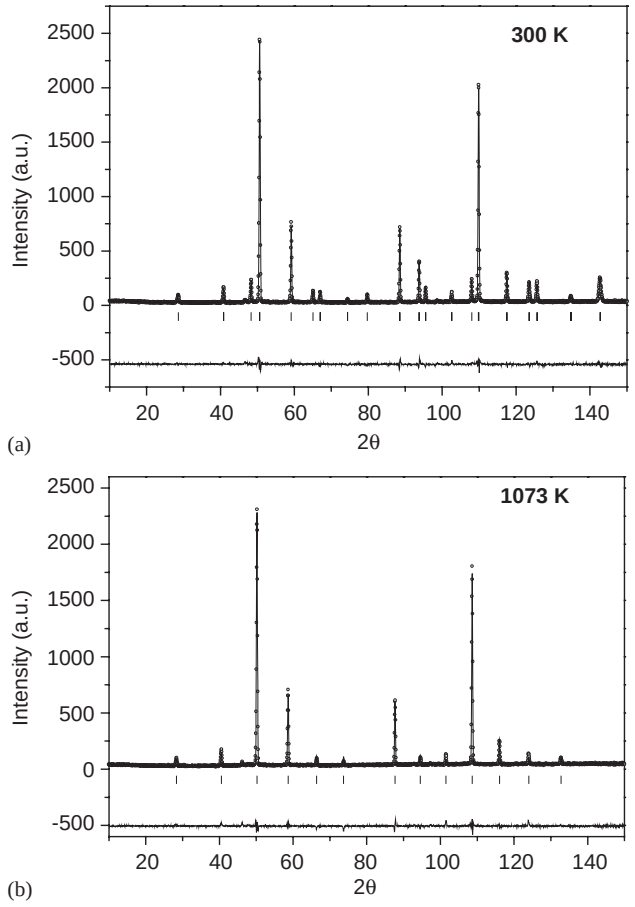

Fig. 2. Refined neutron powder diffraction patterns of $Li_{0.2}Na_{0.3}La_{0.5}TiO_3$ at room temperature (a) and at 1073 K (b). Differences between observed and calculated intensities are shown. Short vertical bars denote expected Bragg positions.

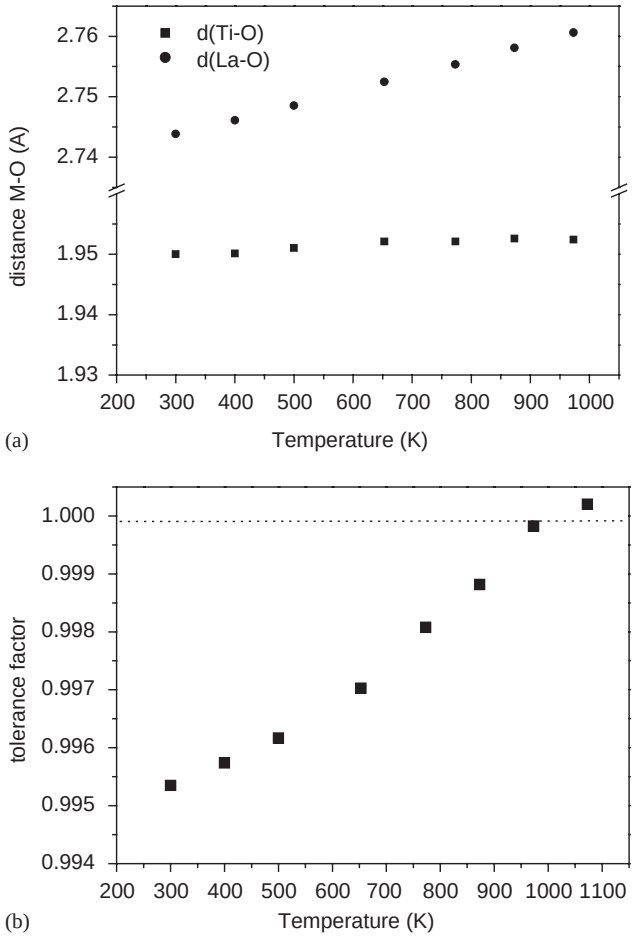

Fig. 3. (a) Evolution of La(Na)–O and Ti–O distances with temperature in the rhombohedral perovskite. (b) Evolution of tolerance factors with the temperature for the $Li_{0.2}Na_{0.3}La_{0.5}TiO_3$ sample.

rhombohedral perovskites [19]. However, expansion of LaO_{12} cubooctahedra increases in the same way a and c parameters, making that c/a ratios do not change with temperature.

On the other hand, superlattice reflections of the rhombohedral phase ($R\bar{3}c$ S.G.) are very sensitive to oxygen positions, which in the last term depend on the octahedral tilting [12]. In this phase, the tilting scheme corresponds to the ($a^-a^-a^-$) type of the Glazer's notation (equal out-of-phase tiltings along three orthogonal directions [20]). At increasing temperatures, the intensity of the superlattice reflections ((113), (125) (315) and (137)) decreases and disappear at 1073 K. The ND pattern of the perovskite heated at 1073 K was indexed with a simple cubic perovskite ($a_p = 3.9085(1)$ Å). In this case, the Space Group is $Pm3m$ and the tilting scheme can be described as ($a^0a^0a^0$) [20]. It is worthwhile to note that detection of the rhombohedral-cubic transition was not possible with our experimental XRD setup, because this phase, was always seen as cubic with this technique [7–11].

During the heating of the sample between 300 and 1073 K, the octahedral tilting decreased from 6.5 to 0° (Fig. 4a). Changes detected in octahedral tilting are small below 773 K but become important above this temperature. In sample heated at 1073 K, the octahedral tilting was completely eliminated. The absence of any discontinuity/slope change in the unit cell volume versus temperature plot, confirms the displacive character of the reversible rhombohedral-cubic transition (Fig. 1b).

In the analyzed temperature range, TiO_6 octahedra are regular (equal Ti–O distances), but La cubooctahedra display appreciable modifications. In the case of the cubic phase, a single La–O distance was detected (2.76 Å), while in the rhombohedral phase, three different distances 2.52, 2.75 and 2.96 Å were observed (Table 3). The distortion of LaO_{12} polyhedra is a consequence of the antiphase tilting of TiO_6 octahedra along the [111] direction, which produces the enlargement of three La–O distances (La–O′ = 2.96 Å) and the shortening of other three distances (La–O″ = 2.52 Å) in the cubooctahedra (Fig. 5). The progressive elimination

Table 3
Evolution of the Ti–O, La–O and O–O, distances (in Å) with temperature; Polyhedra volumes (in Å^3) and octahedral tilt angles, φ (in deg) are also indicated

	300 K	400 C	500 K	650 K	773 K	873 K	973 K	1073 K (C)	
Ti–O	1.946(8)	1.950(2)	1.951(2)	1.952(2)	1.952(3)	1.953(2)	1.952(4)	1.954	Ti–O
⟨La–O⟩	2.742(12)	2.7460(2)	2.748(2)	2.752(2)	2.755(5)	2.758(3)	2.761(6)	2.764	La–O
3 × La–O′	2.9588	2.9511	2.943	2.9241	2.8942	2.8681	2.8025	2.764	3 × La–O′
6 × La–O	2.7474	2.7496	2.7517	2.7551	2.7567	2.7593	2.760	2.764	6 × La–O
3 × La–O″	2.5205	2.534	2.5477	2.5755	2.6138	2.6457	2.7199	2.764	3 × La–O″
V_A[a]	48.60	48.81	48.94	49.15	49.31	49.45	49.59	49.77	V_A
V_B[a]	9.82	9.89	9.90	9.92	9.92	9.93	9.92	9.95	V_B
V_A/V_B[a]	4.95	4.94	4.94	4.96	4.97	4.98	4.997	5.00	V_A/V_B
τ[b]	0.9967	0.9957	0.9962	0.9970	0.9981	0.9988	0.9998	1.0002	τ
φ(°)	6.46	6.2	5.81	5.17	4.19	3.24	1.17	0	φ(°)
(O–O)l	4.195	4.186	4.171	4.145	4.101	4.058	3.96	3.909	(O–O)l
(O–O)s	3.577	3.592	3.613	3.648	3.698	3.746	3.848	3.909	(O–O)s

[a] $V_A = V(LaO_{12}) = (10/3\sqrt{2})(d_{A-O})^3$, $V_B = V(TiO_6) = 4/3(d_{B-O})^3$ (taken from Ref. [21]).
[b] τ = Goldschmidt tolerance factor = $d_{A-O}/\sqrt{2}d_{B-O}$.

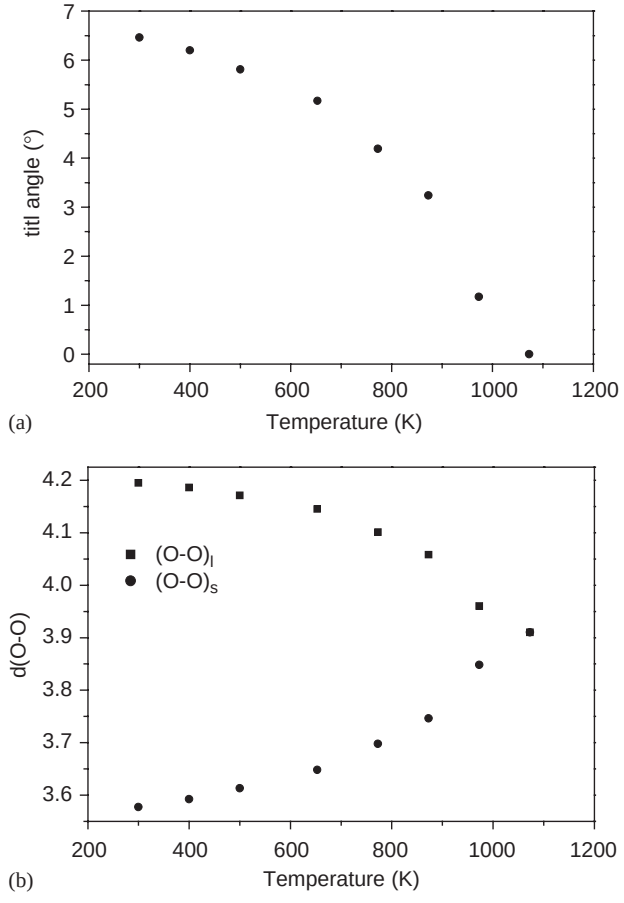

Fig. 4. (a) Temperature dependence of octahedral tilting. (b) Temperature dependence of O–O diagonal distances in square windows that connect contiguous *A*-sites of the perovskite.

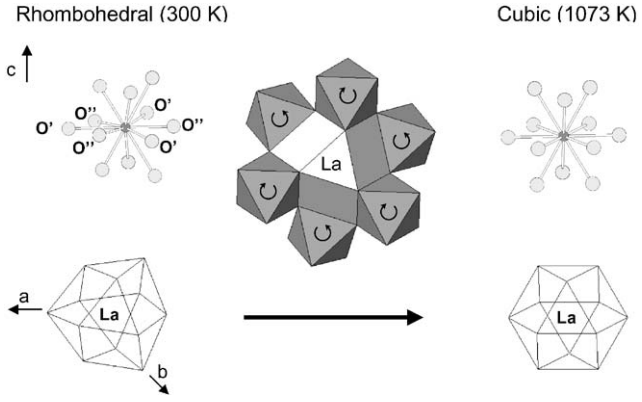

Fig. 5. Changes produced on La cubooctahedra by the elimination of the octahedral tilting in rhombohedral-cubic transformation.

of the octahedral tilting makes that these distances approach that of undistorted polyhedra (2.76 Å). Details about cubooctahedra distortions can be obtained in Fig. 5 and Table 3, where the evolution of La–O distances with temperature is analyzed.

Structural modifications produced along the transition are responsible for the expansion of the *a*-axis. However, expansion detected along the *c*-axis cannot be explained with the elimination of the octahedral tilting. A careful analysis of octahedra revealed that octahedra are slightly distorted (flatened) along the *c*-axis at room temperature (rhombohedral perovskite), but they expand along this axis when temperature increased (cubic phase). During heating the angle formed by Ti–O bonds with the *c*-axis changes from 55° to the ideal 54.75° value. From this fact, it is concluded that expansion of the *c*-axis is due to expansion of octahedra [22].

As a consequence of the elimination of octahedral tilting, distorted rhombic windows that connect contiguous A-sites of the perovskite becomes regular (Fig. 4b). In particular, the two O–O distances detected in the low temperature phase (3.58 and 4.20 Å) becomes a single one (3.90 Å) at high temperatures (1073 K).

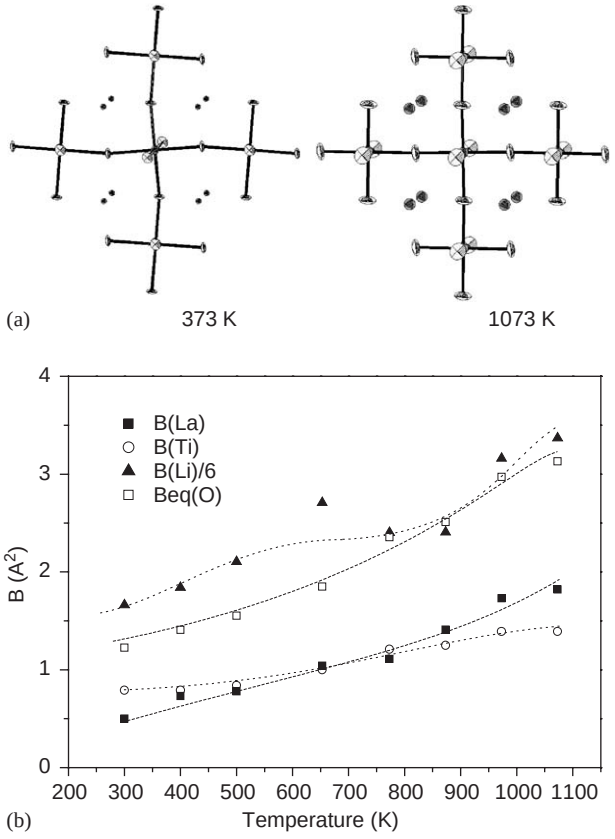

Fig. 6. (a) Atomic thermal displacements at 300 and 1073 K in $Li_{0.2}Na_{0.3}La_{0.5}TiO_3$. Ellipsoids correspond to the anisotropic thermal factors of oxygens. (b) Temperature dependence of isotropic thermal factors of Ti, La/Na, Li and O atoms. For oxygen atoms, equivalent B factors were calculated from the corresponding anisotropic values. For a better analysis, Li values were divided by a factor of 6.

Changes produced in square windows should favor Li mobility; however, vacancies concentration is maintained below the percolation threshold ($0.2 < n_p = 0.31$). According to this fact, ion conductivity is very low in this perovskite ($\leqslant 10^{-7}\,\Omega\,cm^{-1}$ at 600 K), indicating that the long-rang diffusion of lithium is not favored in the $Li_{0.2}Na_{0.3}La_{0.5}TiO_3$.

A comparison of thermal ellipsoids deduced at 300 and 1073 K is given in Fig. 6a. Oxygen thermal factors are clearly anisotropic and local displacements of oxygen atoms along Ti–O bonds are significantly smaller than those produced in perpendicular directions. Oxygen thermal factors are considerably higher than those of titanium ions, suggesting that some oscillation of octahedral around titanium could be produced (Fig. 6b). Taking into account that Li ions are located at the centre of the unit cell faces of the perovksite; Li motion should be favored by octahedral oscillations. The rapid increment detected on Li thermal factors above 773 K suggests that motion of lithium is enhanced at high temperatures.

5. Conclusions

The thermal heating of the rhombohedral $Li_{0.2}Na_{0.3}La_{0.5}TiO_3$ perovskite, produces the isotropic expansion of the unit cell. The Rietveld analysis of ND patterns recorded at increasing temperatures shows that the expansion of the LaO_{12} polyhedra is considerably higher that TiO_6 octahedra. This fact explains the slight increase detected in the tolerance Goldschmidt factor, τ, with temperature. ND pattern of the sample heated at 1073 K corresponds to that of the cubic perovskite.

Above 773 K a reduction of the octahedral tilting along the [111] direction is produced, explaining the rhombohedral-cubic transition detected by ND technique. This transformation produces an appreciable modification of La cubooctahedra and dimensions of square windows that connect contiguous A-sites of the perovskite. This fact should favor Li mobility; however, the existence of a concentration of vacant A-sites lower than the percolation threshold ($0.2 < n_p = 0.31$) limits Li diffusion in the perovskite.

Ackowledgments

Authors thank Drs. J.A. Alonso, C. León, J. Santamaría and M.L. Sanjuán for helpful discussions and ILL for the provision of neutron beam time. We thank the Spanish Agency CICYT (MAT2001-3713-C04-03 projects) for the financial support.

References

[1] A.G. Belous, G.N. Novitskaya, S.V. Polyanetskaya, Y.I. Gornikov, Zh. Neorg. Khim. 32 (1987) 283–286.
[2] Y. Inaguma, L. Chen, M. Itoh, T. Nakamura, T. Uchida, H. Ikuta, M. Wakihara, Solid State Commun. 86 (1993) 689–693.
[3] S. Stramare, V. Thangadurai, W. Weppner, Chem. Mater. 15 (2003) 3974–3990.
[4] M.A. Paris, J. Sanz, C. Leon, J. Santamaría, J. Ibarra, A. Varez, Chem. Mater. 12 (2000) 1694–1701.
[5] A.I. Ruiz, M.L. López, M.L. Veiga, C. Pico, Solid State Ion. 112 (1998) 291–297.
[6] J.L. Fourquet, H. Duroy, M.P. Crosnier-Lopez, J. Solid State Chem. 127 (1996) 283–294.
[7] A.D. Robertson, S. García-Martín, A. Coats, A.R. West, J. Mater. Chem. 5 (1995) 1405–1412.
[8] J.-S. Lee, K.S. Yoo, T.S. Kim, H.J. Jung, Solid State Ion. 98 (1997) 15–26.
[9] Y. Harada, Y. Hirakoso, H. Kawai, J. Kuwano, Solid State Ion. 121 (1999) 245–251.
[10] J. Ibarra, A. Várez, C. León, J. Santamaría, L.M. Torres-Martinez, J. Sanz, Solid State Ion. 134 (2000) 219–228.
[11] A. Várez, J. Ibarra, A. Rivera, C. León, J. Santamaría, M.A. Laguna, M.L. Sanjuán, J. Sanz, Chem. Mater. 15 (2003) 225–232.
[12] J.A. Alonso, J. Sanz, J. Santamaría, C. León, A. Várez, M.T. Fernandez-Diaz, Angew. Chem. Int. Ed. 3 (2000) 619–621.
[13] J. Sanz, J.A. Alonso, A. Várez, M.T. Fernández-Díaz, Dalton Trans. (2002) 1406–1408.

[14] Y. Inaguma, T. Katsumata, M. Itoh, Y. Morii, J. Solid State Chem. 166 (2002) 67–72.
[15] A. Várez, Y. Inaguma, M.T. Fernández-Díaz, J.A. Alonso, J. Sanz, Chem. Mater. 15 (2003) 4637–4641.
[16] J. Sanz, A. Várez, J.A. Alonso, M.T. Fernández-Díaz, J. Solid State Chem. 177 (2004) 1157–1164.
[17] Y. Inaguma, M. Itoh, Solid State Ion. 86–88 (1996) 257–260.
[18] A. Rivera, C. León, J. Santamaría, A. Varez, O. V'yunov, A.G. Belous, J.A. Alonso, J. Sanz, Chem. Mater. 14 (2002) 5148–5152.
[19] H.D. Megaw, C.N.W. Darlington, Acta Crystallogr. A 31 (1975) 161–173.
[20] A.M. Glazer, Acta Crystallogr. B 28 (1972) 3384–3392.
[21] N.W. Thomas, Acta Crystallogr. B 45 (1989) 337–344.
[22] M. O'Keefe, B.G. Hyde, Acta Crystallogr. B 33 (1977) 3802–3813.